J. Fluid Mech. (1979), *vol.* 94, *part* 3, *pp.* 519–540
Printed in Great Britain

Is the Weis-Fogh principle exploitable in turbomachinery?

By S. B. FURBER AND J. E. FFOWCS WILLIAMS
Department of Engineering, University of Cambridge

(Received 26 July 1978 and in revised form 22 January 1979)

Weis-Fogh discovered a remarkable new principle of aerodynamic lift. Hovering wasps exploit the principle and fly with an aerodynamic performance superior in some respects to anything previously known. In this paper we address the question of whether the Weis-Fogh effect can be exploited in turbomachinery. We think the answer is yes.

Normal turbomachinery design is based on the analysis of isolated cascades of blades with steady entry and exit flows. The interactions between adjacent cascades and nonuniformities of the flow are usually regarded as problems which have to be minimized. Unsteadiness gives rise to noise. In this paper we take the opposite view and examine a novel type of turbomachinery stage that depends on the interaction between rotor and stator for its normal operation. The stage exploits the Weis-Fogh principle and has the unusual property that when started from rest it generates a pressure rise without shedding any vorticity into the fluid. We argue that there may be a performance advantage for stages of this new type.

Experiments were done to check the validity of the theoretical model and these are described. The results seem to show that under certain circumstances a strong rotor–stator interaction can result in an improved stage performance, and we suggest that this improvement may be due to the Weis-Fogh effect.

1. Introduction

An aerofoil accelerating from rest initially generates no lift. The lift will arise only as a circulation develops around the aerofoil as vorticity is shed from the trailing edge. The shed vorticity affects the flow at the trailing edge in such a way as to delay further shedding, and hence the development of full lift takes time. A hovering animal that uses an oscillating wing on which circulation of different sign must be developed for succeeding beats will have its performance impeded by this delay, in that the lift impulse generated by each wing beat will be reduced. In his studies of animal hovering motions, Weis-Fogh (1973) observed that one small insect, the chalcid wasp *Encarsia formosa*, overcomes this problem by a remarkable interaction of the two wings; each wing acts as the starting vortex for the other. The heart of the process rests in an essential separation of two wings that are initially in contact. Lighthill (1973) has given a mathematical analysis of the Weis-Fogh effect and shown how the performance of the wing system is governed by parameters quite different from those determining the forces on conventionally operating isolated aerofoils.

While considering whether this interaction process might have any application in turbomachinery, it is clear that the provision for rapid changes in blade circulations might be particularly relevant to tangential flow fans (see, e.g., Coester 1959). There the

0022–1120/79/4322–7650 $02.00

blade circulation must change twice per revolution, and this is in practice achieved by interaction with the surrounding duct structure.

We think that the operation of these fans has aspects with distinct similarity to the Weis-Fogh principle, and we shall pursue that analogy in due course. But first we need a much simpler flow geometry on which the likely magnitude of the effect can be quantified and checked experimentally.

The main reason that we are seeking an application of the Weis-Fogh effect for turbomachinery is that we expect a performance advantage over conventional systems. We base our expectation solely on the known performance of insects exploiting this principle. The *Encarsia formosa*'s mean lift coefficient whilst airborne, calculated on the assumptions of normal hovering, is 3 (see Weis-Fogh 1973), an exceptionally high value. The basic process includes a mechanism which delays the onset of stall and allows higher circulations to exist. If this can be exploited on turbomachinery blades there could result a significant practical advantage over conventional machinery designed on the aerodynamic principles of non-interacting elements.

The model of the insect's wing motions studied by Lighthill is based on aerofoils rotating about a span-wise axis. Though this may well have future relevance to tangential flow fans we are seeking first a scheme that might be used for axial flow machinery in which rotating cascades of blades move parallel to adjacent static cascades. For that we choose a new model in which aerofoils, whose relative motion is purely translational, interact as a result of their proximity during part of the motion.

Of course the geometry has to be simplified for an exact analysis to be tractable, and at least initially all viscous effects must be ignored. The same was true for Lighthill's successful modelling of the Weis-Fogh insect motion. Since we might expect viscous terms to be even smaller at the much higher Reynolds number that will be of engineering interest in real machines, we anticipate that our model will be representative of the real flow. Furthermore, as Lighthill (1973) points out, in this radically unconventional method of producing lift viscous terms can actually be beneficial and augment the lifting ability of the wings.

Also for the sake of simplicity we begin by examining in isolation a single pair of interacting aerofoils. This is the fundamental and simplest geometry in which the principle can be demonstrated. Cascade results will follow later. Isolated aerofoil analysis furnishes the same canonical problem for conventional cascades. The essence of our application of the Weis-Fogh principle is that the rotor and stator blades should pass close enough that they are effectively in contact for a finite part of the blade to blade period. The circulation on an individual rotor blade after it has left contact with the stator, and which determines its lift, is set by the potential flow about the composite deforming two-blade body at the instant prior to separation. We determine this flow by conformal transformation.

Our analytical results confirm that the Weis-Fogh principle is applicable to geometrical configurations suitable for turbomachinery applications. We show that the force on blades operating at similar angles of incidence is of the same order regardless of whether they are operating in the conventional or in the Weis-Fogh mode. But we expect that, just in the same manner as that practised by the chalcid wasp, much higher stall-free incidences are made possible by the strong unsteady blade to blade interactions of the Weis-Fogh effect. It is in that area that we would expect significant advantage over conventional machines. Our experiment tends, we think, to confirm this view.

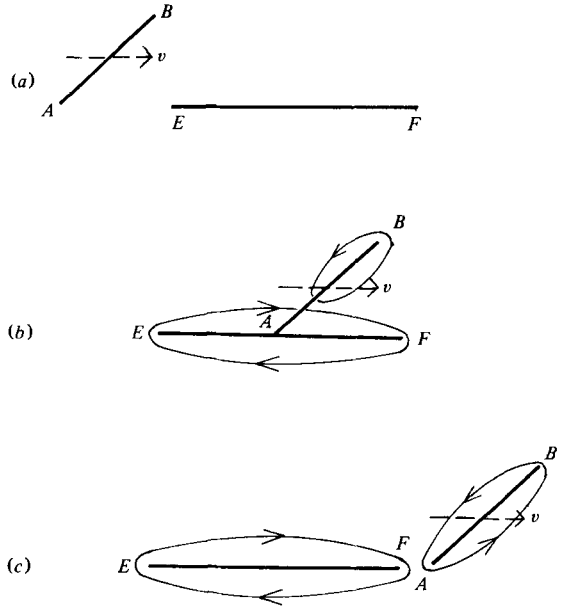

FIGURE 1. The physical plane. The rotor AB moves with a velocity v parallel to the fixed stator EF. The blades are in an external flow with velocity components (U, V) at infinity, and the total circulation on the system is C.

2. The flow around interacting aerofoils

Our model consists of a rotor blade AB and a stator blade EF, each represented by a flat plate (figure 1). The stator is aligned parallel to the direction of motion of the rotor, and the trailing edge of the rotor maintains contact with the upper surface of the stator while the blades pass.

We chose this model because it represents a situation where the Weis-Fogh effect might operate in a geometry not unrepresentative of an axial compressor stage. Also it is possible to calculate analytically full details of the flow field using potential flow theory, at least for that part of the motion when the blades are in contact. The problem is unusual in that the boundary is deforming, and eventually splitting into two disconnected bodies. A potential flow, however, does not depend on the history of the boundaries, but only on the instantaneous boundary velocities. Thus rather than analysing the problem with a moving physical rotor, we may consider the equivalent problem where AB in figure 1 is a fixed boundary on which a normal velocity is prescribed. This then allows us to transform the boundary by conformal mapping into something more easily handled. The flow region in figure 1 may be considered to be the exterior of a polygon, and this may be transformed into the exterior of the unit circle (Jeffreys & Jeffreys 1956, §13-094) *via* the conformal mapping

$$\frac{dz}{d\zeta} = K\zeta^{-2}\left(\frac{\zeta-\zeta_{a_2}}{\zeta-\zeta_{a_1}}\right)^{\alpha/\pi}\left(\frac{\zeta-\zeta_b}{\zeta-\zeta_{a_2}}\right)(\zeta-\zeta_e)(\zeta-\zeta_f), \tag{2.1}$$

where α is the angle of incidence of the rotor, K is a scaling constant, and ζ_b is the mapping of B into the ζ-plane, etc. Note that, since the polygon in the z-plane is degenerate, the trailing edge of the rotor (A) corresponds to two vertices, which transform distinctly into ζ_{a_1} on EAB and ζ_{a_2} on BAF (figure 2).

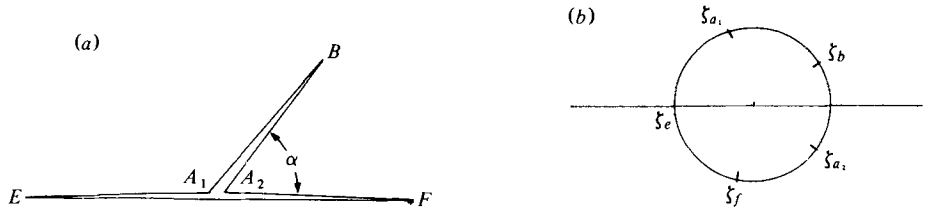

FIGURE 2. The conformal transformation. (*a*) The z-plane. The physical boundary may be thought of as a degenerate polygon. (*b*) The ζ-plane. The boundary in the z plane may be transformed into the unit circle in the ζ-plane via equation (2.1).

This transformation enables us to find a complex potential, and hence full details of the flow field, but first it is relevant to consider the geometrical details of the transformation.

We want $z(\zeta)$ to be single valued, and this requires that the coefficient of ζ^{-1} in the expansion of equation (2.1) in negative powers of ζ be zero. This gives the following interrelation between the values of ζ at the transformed vertices:

$$(\alpha/\pi)(\zeta_{a_2}-\zeta_{a_1})+\zeta_f+\zeta_b+\zeta_e-\zeta_{a_2}=0. \tag{2.2}$$

We are free to prescribe any value on the unit circle for one of the transformed vertices, and here we take $\zeta_e = -1$.

Other values correspond to rotations of the boundary in the ζ-plane. Then we may take any values consistent with equation (2.2) for the other transformed vertices, in sequence round the unit circle, and use them to integrate equation (2.1) numerically to obtain the various lengths in the physical plane.

As the rotor moves across the stator, the transformed vertices move around the unit circle in a manner which is hard to establish by anything other than numerical methods.

The complex potential may be considered as the linear superposition of three components; the flow generated by the relative motion of the blades, that caused by an external stream, and that caused by a non-zero total circulation on the system. All three may be evaluated, and we look first at the component generated by the relative motion of the blades with zero total circulation and no flow at a large distance.

The motion of the rotor is represented by a normal velocity boundary condition in the physical plane, and, since the normal velocity is equal to the derivative along the boundary of the stream function ψ, we may express the boundary conditions as

$$\psi = \begin{cases} -v\sin\alpha\, z\, e^{-i\alpha} & \text{on the rotor} \\ 0 & \text{on the stator} \end{cases} \tag{2.3}$$

provided that we take the trailing edge A of the rotor at $z = 0$.

The boundary conditions may be transferred into the ζ-plane, where they become

$$\psi = \begin{cases} -v\sin\alpha\, e^{-i\alpha} z(e^{i\eta}) & \text{for } \eta_{a_1} > \eta > \eta_{a_2}, \\ 0 & \text{otherwise,} \end{cases} \tag{2.4}$$

where $\zeta = e^{i\eta}$ on the unit circle. The corresponding complex potential is

$$\omega(\zeta) = -\frac{v\sin\alpha}{\pi}\int_{\zeta_{a_1}}^{\zeta_{a_2}} \frac{z(\zeta')\, e^{-i\alpha}}{(\zeta-\zeta')}\, d\zeta', \tag{2.5}$$

where the integration is to be taken clockwise round the unit circle, and the trailing edge of the rotor is taken at the origin in the physical plane ($z(\zeta_{a_1}) = 0$).

This is the complex potential for the flow generated by the relative motion of the rotor and stator. The total complex potential will include contributions representing an external flow and a non-zero total circulation. These are easily calculated, since the boundary in the ζ-plane is a circle. An external stream with velocity (U, V) at a large distance in the z-plane gives rise to a complex potential

$$\omega_e(\zeta) = (U+iV)\zeta K + (U-iV)\zeta^{-1}\bar{K}, \tag{2.6}$$

where the overbar denotes the complex conjugate, and a total circulation C adds

$$\omega_C(\zeta) = \frac{iC}{2\pi}\log\zeta. \tag{2.7}$$

Thus the complex potential is known for any flow condition.

If in the z-plane an external stream is applied with the same velocity as the rotor, so $(U, V) = (v, 0)$ and $C = 0$, it is clear that a uniform flow parallel to the stator will result. Thus

$$\zeta K + \zeta^{-1}\bar{K} - \frac{\sin\alpha}{\pi}\int_{\zeta_{a_1}}^{\zeta_{a_2}} \frac{z\,e^{-i\alpha}}{(\zeta-\zeta')}\,d\zeta' = z. \tag{2.8}$$

Hence equation (2.5) may be written in the following form which is more convenient for computation:

$$\omega(\zeta) = v(z - \zeta K - \zeta^{-1}\bar{K}). \tag{2.9}$$

The complex potential with external flow (U, V) and circulation C is then

$$\begin{aligned}\omega_T &= \omega + \omega_e + \omega_c \\ &= vz + (U-v+iV)\zeta K + (U-v-iV)\zeta^{-1}\bar{K} + \frac{iC}{2\pi}\log\zeta.\end{aligned} \tag{2.10}$$

We now have full information on the flow around our simple two blade model immersed in any external flow, for the period while the blades are in contact. This will enable us to calculate the forces on the blades, and see how the interaction will affect the blade circulations. We can then use the results to estimate the performance of cascades of interacting blades, treating each interaction between two blades in isolation as a first approximation, and compare with the performance of a conventional stage.

The complex potential in equation (2.10) may be used with the conformal transformation [equations (2.1) and (2.2)] to calculate the streamlines for any geometry and flow condition. Since the conformal transformation is written in terms of ζ it is natural to start in the ζ-plane. The boundary in the ζ-plane is a circle, and therefore polar coordinates with the origin at the centre of the circle were chosen. One hundred values of each co-ordinate were taken to cover an annular region from the boundary to a circle six times the radius of the boundary, and figure 3(a) shows the co-ordinate system for every fifth value taken.

Suitable positions for the transformed vertices on the unit circle were then chosen to give a rotor of equal length to the stator, and inclined at 45° to it, with the two blades about to separate (A and F coincident in figure 1). Equation (2.1) was integrated round the unit circle in the ζ-plane to give the value of z corresponding to each of the one

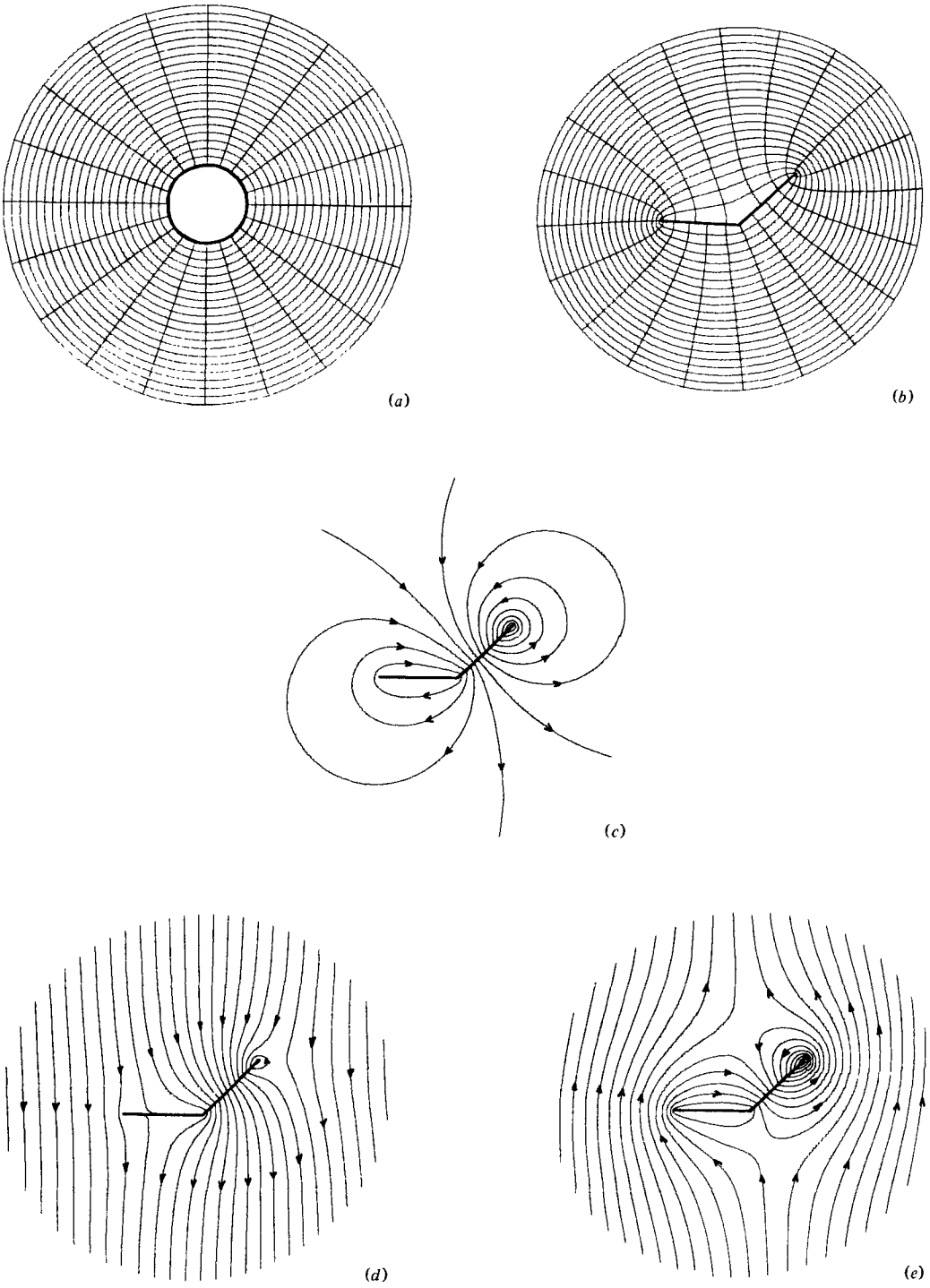

FIGURE 3. (*a*) The co-ordinate system in the ζ-plane, showing every fifth value. (*b*) The co-ordinate system of (*a*) transformed into the z-plane. (*c*) Streamlines for the flow generated by rotor motion alone, showing clearly the circulatory motion. (*d*) A descending stream, with $\frac{1}{4}$ of the rotor velocity, has been added to the flow of (*c*); this corresponds to an axial flow with no swirl in a conventional machine. (*e*) An ascending stream is added to the flow of (*c*), and the blade circulations are augmented.

hundred chosen values of ζ on the boundary. These values of z could then be used as starting points for integrating equation (2.1) along each of the radial lines in the ζ-plane, and the map of all the chosen values of ζ onto the z-plane found. The method of integration used for both of the preceding steps was that of taking the derivative midway between two adjacent points in the ζ-plane as an approximation to the gradient of the chord joining the points, except at A_1 and A_2 in figure 2 where a local approximation is needed to calculate adjacent points on the boundary. The results of this numerical mapping are shown in figure 3(*b*) which gives the transformation into the z-plane of the co-ordinates shown in figure 3(*a*) in the ζ-plane.

Once corresponding values of z and ζ are known, it is straightforward to calculate the value of the stream function $\psi = \mathrm{Im}\,(\omega)$ from equation (2.10) at each position for any required flow condition. These values were then fed to a contour plotting routine, along with the set of z or ζ values, and the streamlines in the corresponding plane were output.

Figure 3(*c*) gives the streamlines in the absence of any external flow or net circulation, and shows clearly the circulation developed around the rotor leading edge, and in the opposite direction around the stator. When an external stream approaches vertically from above with one quarter of the rotor's velocity, the streamlines are as shown in figure 3(*d*). The circulation on the rotor is partly cancelled by the streaming around the body, but some remains. This has been established by a procedure to be described later in this section. If the external flow approaches instead from vertically below the circulation is enhanced. The streamlines for this flow are shown in figure 3(*e*). There are now two saddle-points in the flow away from the boundary.

The complex potential [equation (2.10)] also contains sufficient information to work out all the pressure distributions, but an evaluation of the overall lift generating performance may be obtained more directly from consideration of the blade circulations. We consider the case where there is no external stream, and the flow is generated solely by the rotor motion. We take also zero total circulation, corresponding to starting the motion from rest in a stationary fluid. Under these conditions, the circulations generated on the rotor and stator will be equal and opposite.

The velocity is the gradient of the velocity potential, so the circulation round a curve is the change in the potential going once round the curve. The circulation on the rotor is therefore the change in the potential across the trailing edge

$$\Gamma = \mathrm{Re}\,[\omega(\zeta_{a_1}) - \omega(\zeta_{a_2})], \tag{2.11}$$

taking an anti-clockwise circulation in figure 1 as positive. Thus from equation (2.10)

$$\Gamma = v\,\mathrm{Re}\,[K(\zeta_{a_1} - \zeta_{a_2}) + \bar{K}(\zeta_{a_1}^{-1} - \zeta_{a_2}^{-1})]. \tag{2.12}$$

This equation gives the circulation on the rotor at any time when the blades are in contact. What happens when the blades are not in contact? We know from Kelvin's circulation theorem that vorticity is conserved in incompressible inviscid two-dimensional flow, and it follows that the circulation on either blade cannot change once they are separated. Thus the circulations carried by the blades between contacts are determined entirely by the conditions around the blades at the time of separation. For our calculations we take the circulation after separation to be equal to that on the blade immediately prior to separation; we justify this in § 3.

At the moment of separation the geometry is determined by the angle of incidence of the rotor, the ratio of the length of the rotor to that of the stator, and a scale factor. The circulation on the rotor may be compared with the Kutta circulation at the same angle of incidence, and the ratio will depend only on the first two factors above. It may be calculated as follows.

At separation A and F coincide, so $\zeta_{a_2} = \zeta_f$ and equation (2.2) reduces to

$$\frac{\alpha}{\pi}(\zeta_{a_2} - \zeta_{a_1}) + \zeta_b - 1 = 0. \tag{2.13}$$

Since the transformed vertices are on the unit circle we may write

$$\zeta_b = \exp(i\eta_b), \quad \zeta_{a_1} = \exp(i\eta_{a_1}), \quad \zeta_{a_2} = \exp(i\eta_{a_2}), \tag{2.14}$$

whereupon equation (2.13) becomes two real equations

$$\begin{aligned} &\frac{\alpha}{\pi}(\cos\eta_{a_2} - \cos\eta_{a_1}) + \cos\eta_b - 1 = 0, \\ &\frac{\alpha}{\pi}(\sin\eta_{a_2} - \sin\eta_{a_2}) + \sin\eta_b = 0. \end{aligned} \tag{2.15}$$

We write equation (2.15) in terms of the half angles, and the requirement that the transformed vertices are in the correct sequence round the unit circle leads to

$$\eta_{a_1} + \eta_{a_2} = \eta_b$$

and that either

$$\eta_{a_1} - \eta_{a_2} = 2\sin^{-1}((\pi/\alpha)\sin\tfrac{1}{2}\eta_b)$$

or

$$\eta_{a_1} - \eta_{a_2} = 2\{\pi - \sin^{-1}((\pi/\alpha)\sin\tfrac{1}{2}\eta_b)\}. \tag{2.16}$$

Equations (2.16) have valid solutions only when $0 \leqslant \eta_b \leqslant 2\sin^{-1}(\alpha/\pi)$ and when this is satisfied they yield two possible solutions for η_{a_1} and η_{a_2}.

On the unit circle $\zeta = e^{i\eta}$ we may write equation (2.1) in terms of the half angles:

$$\frac{dz}{d\eta} = K'\left\{\frac{\sin\tfrac{1}{2}(\eta - \eta_{a_2})}{\sin\tfrac{1}{2}(\eta - \eta_{a_1})}\right\}^{\alpha/\pi} \sin\tfrac{1}{2}(\eta - \eta_b)\cos\tfrac{1}{2}\eta, \tag{2.17}$$

where

$$K' = 4K\exp(\tfrac{1}{2}i\{[\eta_{a_2} - \eta_{a_1}]\alpha/\pi + \eta_b\}),$$

which is real. Equation (2.17) may be integrated numerically using values for η_{a_1}, η_{a_2} and η_b found as described above to give the rotor and stator lengths. The circulation may be found from equation (2.12) and compared with the Kutta circulation. The results of these calculations are shown in figure 4, which gives the ratio of the interaction circulation to the Kutta circulation against the ratio of the rotor length to the stator length for various values of α, the rotor angle of incidence.

Figure 5 gives the rotor lift coefficient against angle of incidence for various ratios of rotor to stator length near unity, and also, for comparison, the Kutta lift coefficient.

Although it was found necessary to use a computer to integrate equation (2.17) for general cases, the asymptotic behaviour of the ratio of circulations shown in figure 6 may be calculated for ratios of blade lengths either much greater or much less than unity, as may the rate of increase of lift coefficient with angle of incidence in figure 5 when the angle of incidence is near zero.

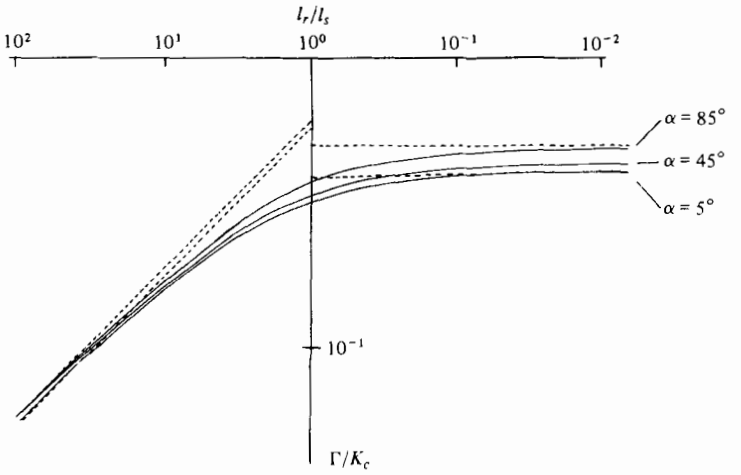

FIGURE 4. The results of theoretical calculations. The ratio of the circulation Γ imparted by the interaction to that K_c imposed by the Kutta condition against the ratio of the rotor length l_r to the stator length l_s for various rotor angles of incidence α, with the asymptotic values for $\alpha = 0°$ or $90°$ and $l_r/l_s \gg 1$ or $l_r/l_s \ll 1$ shown dotted.

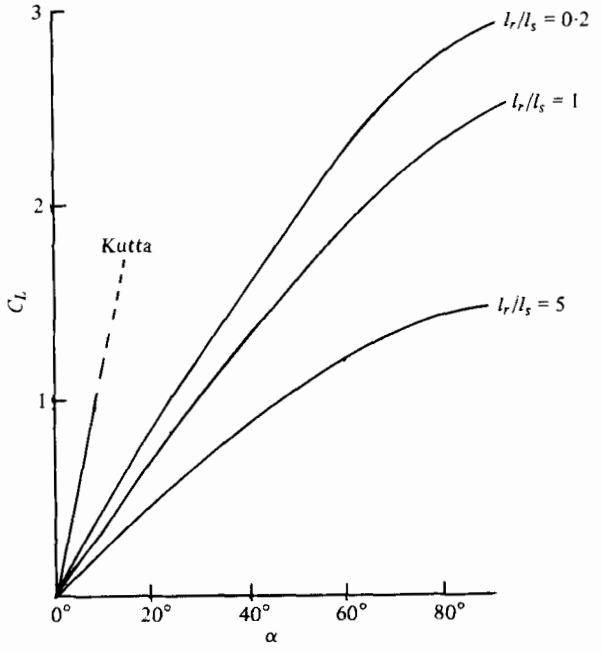

FIGURE 5. The results of theoretical calculations. The rotor lift coefficient C_L generated by the interaction is plotted against the rotor angle of incidence α for various ratios of rotor length l_r to the stator length l_s. The lift coefficient resulting from application of the Kutta condition in the absence of the stator is also shown.

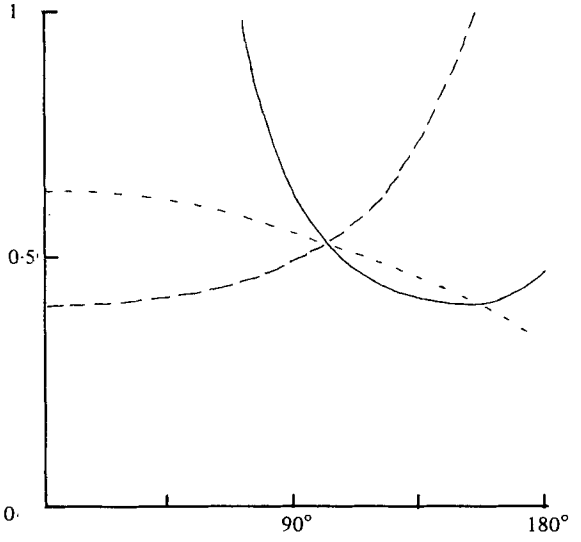

FIGURE 6. $I(\alpha)$ as defined by equation (2.29) is shown for values of α from 0° to 180°, together with $\{2\alpha \sin\alpha\, I(\alpha)\}^{-1}$ (broken line) and $\{2\alpha^2 I(\alpha)\}^{-\frac{1}{2}}$ (dotted). These last two curves represent the α dependence of the asymptotes given by equations (2.28a) and (2.28b).

When the rotor is much smaller than the stator, equations (2.16) reduce to

$$\begin{aligned} \eta_{a_1} + \eta_{a_2} &= \eta_b, \\ \eta_{a_1} - \eta_{a_2} &= (\pi/\alpha)\,\eta_b, \end{aligned} \tag{2.18a}$$

whereas when the stator is much larger than the rotor they become

$$\begin{aligned} \eta_{a_1} + \eta_{a_2} &= \eta_b, \\ \eta_{a_1} - \eta_{a_2} &= 2\pi - (\pi/\alpha)\,\eta_b. \end{aligned} \tag{2.18b}$$

In either case the length of the larger blade is approximately independent of the length of the smaller blade, and may be found by setting $\eta_{a_1} = \eta_{a_2} = 0$ in equation (2.17). Then

$$dz/d\eta = K' \tfrac{1}{2} \sin\eta \tag{2.19}$$

and so the length of the larger blade is

$$\int_{\pi}^{0} \frac{dz}{d\eta}\, d\eta = K'. \tag{2.20}$$

The length of the smaller blade may be found by approximating (2.17) to

$$\frac{dz}{d\eta} = \tfrac{1}{2} K' \left(-\frac{\eta - \eta_{a_2}}{\eta - \eta_{a_1}} \right)^{\alpha/\pi} (\eta - \eta_b), \tag{2.21}$$

which is valid for a small rotor over the range of integration necessary to find the rotor length:

$$l_r = -\int_{\eta_{a_2}}^{\eta_b} \tfrac{1}{2} K' \left(-\frac{\eta - \eta_{a_2}}{\eta - \eta_{a_1}} \right)^{\alpha/\pi} (\eta - \eta_b)\, d\eta, \tag{2.22}$$

and a similar expression may be found for the stator length when it is much smaller than the rotor. Equations (2.18a, b) may be used to find the dependence in equation (2.22) of l_r on η_b, and this may be written as

$$l_r = \tfrac{1}{2} K' \eta_b^{\alpha/\pi} \int_t^1 \left(\frac{t-x}{x-u} \right)^{\alpha/\pi} (1-x)\, dx, \tag{2.23}$$

where $2t = (1-\pi/\alpha)$ and $2u = (1+\pi/\alpha)$, or more compactly as

$$l_r = \tfrac{1}{2}K'\eta_b^2 I(\alpha). \tag{2.24}$$

Equation (2.12) gives the interaction-induced circulation, which may be approximated when either blade is small. For the small rotor

$$\arg K = 0 \tag{2.25a}$$

and for the small stator

$$\arg K = \alpha - \eta_b. \tag{2.25b}$$

So from equation (2.12) for the small rotor

$$\begin{aligned}\Gamma &= \frac{vK'}{2}(\cos\eta_{a_2} - \cos\eta_{a_1}) \\ &= \frac{vK'}{4}\frac{\pi}{\alpha}\eta_b^2,\end{aligned} \tag{2.26a}$$

and similarly for the small stator

$$\Gamma = \frac{v}{4}\frac{\pi}{\alpha}K'\{\eta_b\cos\alpha + 2\sin\alpha\}\eta_b. \tag{2.26b}$$

In all cases the Kutta circulation used for comparison is given by

$$K_c = \pi l_r v \sin\alpha. \tag{2.27}$$

We may now establish the asymptotic forms of the curves in figure 6. For $l_r \ll l_s$ from equations (2.24), (2.26*a*) and (2.27)

$$\Gamma/K_c = \{2\alpha\sin\alpha\, I(\alpha)\}^{-1}, \tag{2.28a}$$

which depends only on an α, and for $l_r \gg l_s$ using equations (2.20), (2.24), (2.26*b*) and (2.27)

$$\Gamma/K_c = \frac{1}{\alpha}\{2(l_r/l_s)\, I(\alpha)\}^{-\frac{1}{2}}. \tag{2.28b}$$

These results give the gradients shown in figure 6 for the two asymptotic conditions. The values may be confirmed if the function

$$I(\alpha) = \int_t^1 \left(\frac{t-x}{x-u}\right)^{\alpha/\pi}(1-x)\,dx, \tag{2.29}$$

where

$$t = \tfrac{1}{2}(1-\pi/\alpha), \quad u = \tfrac{1}{2}(1+\pi/\alpha)$$

is known. It can be shown that

$$I(\alpha) = \left(\frac{\pi}{\alpha}\right)^2\left\{\frac{1+\alpha/\pi}{2}\right\}^{(1+\alpha/\pi)}(2+\alpha/\pi)\,{}_2F_1\left(\frac{\alpha}{\pi}, 1+\frac{\alpha}{\pi}; 3+\frac{\alpha}{\pi}; \frac{1}{2}\left(1+\frac{\alpha}{\pi}\right)\right), \tag{2.30}$$

where

$${}_2F_1(a, b; c; z)$$

is the Gauss hypergeometric function (see Abramowitz & Stegun 1964, chapter 15). A particular case that may be calculated is the limit as α, the rotor angle of incidence, tends to zero. From equation (2.29) we obtain

$$I(0) = \tfrac{1}{8}\pi^2/\alpha^2 \tag{2.31}$$

so for the small rotor

$$\Gamma/K_c \to 4/\pi^2, \tag{2.32a}$$

and for the small stator

$$\Gamma/K_c \to \frac{2}{\pi}(l_r/l_s)^{-\frac{1}{2}}. \tag{2.32b}$$

In general the evaluation of $I(\alpha)$ must be done numerically, and the results are shown in figure 6, along with the corresponding asymptotic values from equation (2.28a), and the intersection with the $\log(l_r/l_s) = 0$ axis of equation (2.28b). The asymptotes for $\alpha = 0°$ and 90° are shown in figure 4. The closeness of these asymptotes reflects the nearly constant nature of $\alpha \sin\alpha\, I(\alpha)$ and $\alpha^2 I(\alpha)$ as shown in figure 6. The lift coefficient in figure 5 is related to the blade circulation by

$$C_L = 2\Gamma/vl_r \tag{2.33}$$

and the dependence on α may be found for small α when the rotor and stator lengths are equal. When $l_r = l_s$,

$$\eta_b = 2\alpha/\pi \tag{2.34}$$

and so from equations (2.16)

$$\eta_{a_1} = \pi/2 + \alpha/\pi$$

and

$$\eta_{a_2} = -\pi/2 + \alpha/\pi. \tag{2.35}$$

From equation (2.12) using the definition of K' in equation (2.17)

$$\Gamma = \frac{vK'}{2}\,\mathrm{Re}\{\exp[-\tfrac{1}{2}i\{(\eta_{a_2} - \eta_{a_1})\alpha/\pi + \eta_b\}]\,(\zeta_{a_2} - \zeta_{a_1})\} \tag{2.36}$$

or in view of equations (2.34) and (2.35)

$$\Gamma = vK' \sin\tfrac{1}{2}\alpha. \tag{2.37}$$

For α near zero and $l_r = l_s$

$$l_r = l_s = \tfrac{1}{2}K' \tag{2.38}$$

and so equation (2.33) becomes

$$C_L = 2\alpha. \tag{2.39}$$

This is in agreement with the initial gradient of the appropriate curve in figure 5. When the rotor and stator lengths are not equal the calculation is more difficult. The model is symmetrical in $\alpha = 0$, so η_b/α will be stationary with respect to small variations in α near zero, and the following may be shown:

if

$$\eta_b = 2k\alpha/\pi,$$

and l_r/l_s is denoted by R:

for $\alpha \ll 1$ and $R \leqslant 1$,

$$R = \frac{1-(1-k^2)^{\frac{1}{2}}}{1+(1-k^2)^{\frac{1}{2}}} \tag{2.40}$$

and

$$C_L = \frac{4k\sin^{-1}k}{\pi[1-(1-k^2)^{\frac{1}{2}}]}\alpha;$$

for $\alpha \ll 1$ and $R \geqslant 1$

$$R = \frac{1+(1-k^2)^{\frac{1}{2}}}{1-(1-k^2)^{\frac{1}{2}}} \tag{2.41}$$

and

$$C_L = \frac{4k(\pi - \sin^{-1} k)}{\pi[1 + (1-k^2)^{\frac{1}{2}}]}\alpha.$$

Hence, the initial gradients of all the curves in figure 5 may be found.

The circulations developed by this interaction are actually slightly lower than those imposed by the Kutta condition at the same incidence, but they are of the same order of magnitude, and the Kutta circulation is not attainable at the higher incidences owing to flow separation. *Encarsia formosa* uses the interaction to generate circulations twice as high as those generated by hovering insects which rely on the Kutta condition, and it therefore seems reasonable to expect that higher circulations are possible with our machine also. What can be achieved in practice will be established only by experiment.

The geometry required for the interaction to generate circulation is not too different from conventional aerofoil designs, and a hybrid machine is possible. The subject of our experiment was such a machine. Moving the rotor blades close to the stator blades in a conventional machine would result in a similar interaction to that presented here, though the approximate rotor–stator seal would exist only for a very short time. The circulation on the blades could be sustained by the interaction to extend stall-free operation under heavy loading.

We have now established that our model geometry will generate a circulation of sufficient magnitude to be of interest, and we can calculate the effect of any of the external flow parameters. We have shown that the interaction principle employed by the wasp may be built into different geometries more suitable for engineering applications, and we suggest that there will be such applications where blading designed to use interactions constructively will give a higher performance than conventional designs.

3. Blade contact and separation

An unusual feature of the flow we are analysing here is that the boundary is not topologically continuous with respect to time. Before the blades touch there are two separate rigid bodies in relative motion, then there is one deforming body, and after separation two rigid bodies again. Unfortunately we have found no way of obtaining an exact solution to the problem when the bodies are not in contact, but certain properties of the flows may be deduced from the laws of potential flow.

We shall demonstrate here that the assumption of the last section, namely that the rotor circulation is the same immediately after separation as it was just before, is a reasonable one. But first let us consider what happens when a rotor approaches a stator.

Suppose that neither blade has any circulation on it, so the system may have been started from rest. While the blades are still some distance apart their flow fields will be approximately independent, and in the rest frame of the stator the total flow pattern will resemble figure 7 (*a*). As the rotor approaches the stator its flow field will be deformed by the presence of the stator. The circulation on each blade cannot change, however, so a very high fluid velocity must be generated through the gap in the final moments before contact. The streamline pattern will be similar to that in figure 7 (*b*). At contact the flow must be suddenly modified to that in figure 7 (*c*) in which there is no

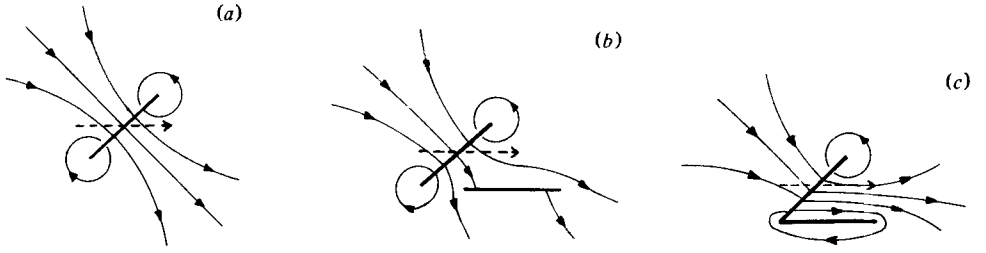

FIGURE 7. (a) The flow generated by a moving rotor distant from the stator with no circulation on either blade. (b) The flow of (a) modified by the proximity of the stator. There is still no circulation on either blade. (c) The flow after blade contact showing the circulations generated on the blades.

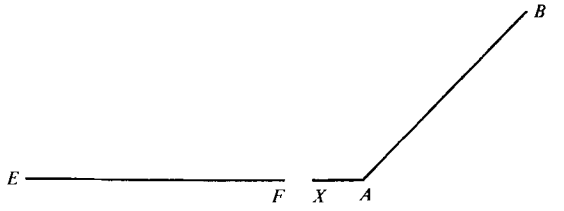

FIGURE 8. The modification for the continuity argument. A small horizontal section AX is added to the trailing edge of the rotor to move the pressure singularity at A away from the gap. The flow local to the initial, vanishingly small gap is then that through an aperture in an infinite plane boundary with the appropriate velocities parallel to the plane prescribed.

flow between the blades. Accompanying this sudden change in the flow pattern is the generation of non-zero circulation on each of the blades, which may be calculated by the methods of the last section.

Thus we see that at blade contact the effective blade circulations are suddenly changed as the irrotational flow of fluid between the blades is cut off. We now consider what happens to the blade circulations when they separate.

Once the blades are separated, by however small a gap, the conditions for Kelvin's circulation theorem are satisfied (Batchelor 1967, §5.2); but at the instant of separation they are not. In particular, the pressure is not single valued at the trailing edge of the rotor. The flow will therefore change instantaneously when a gap appears.

Not only is the pressure not single valued at the rotor trailing edge, but also it is singular on the lower side, as is always the case for flow round a sharp corner. To simplify analysis of the effect of a small gap on the flow, we move the gap away from the corner by adding a small horizontal section to the rotor at the trailing edge (figure 8). The flow near the vanishingly small gap is then approximately the flow through an aperture in a plane boundary with different fluid velocities parallel to the plane on either side. An analysis of the flow will show us how the circulation on each aerofoil is determined at the instant of separation by the asymptotic small gap local flow; once so determined it is preserved in accordance with Kelvin's theorem.

The complex potential for such a flow is

$$\omega = \tfrac{1}{2}(U_1+U_2)\,z+\tfrac{1}{2}(U_1-U_2)\,(z^2-\delta^2)^{\frac{1}{2}}+A\log\left[z+(z^2-\delta^2)^{\frac{1}{2}}\right], \tag{3.1}$$

taking cuts in the z-plane from $-\infty$ to $-\delta$ and from δ to $+\infty$ along the real axis. This gives the potential flow caused by a gap of width 2δ in an infinite plane boundary

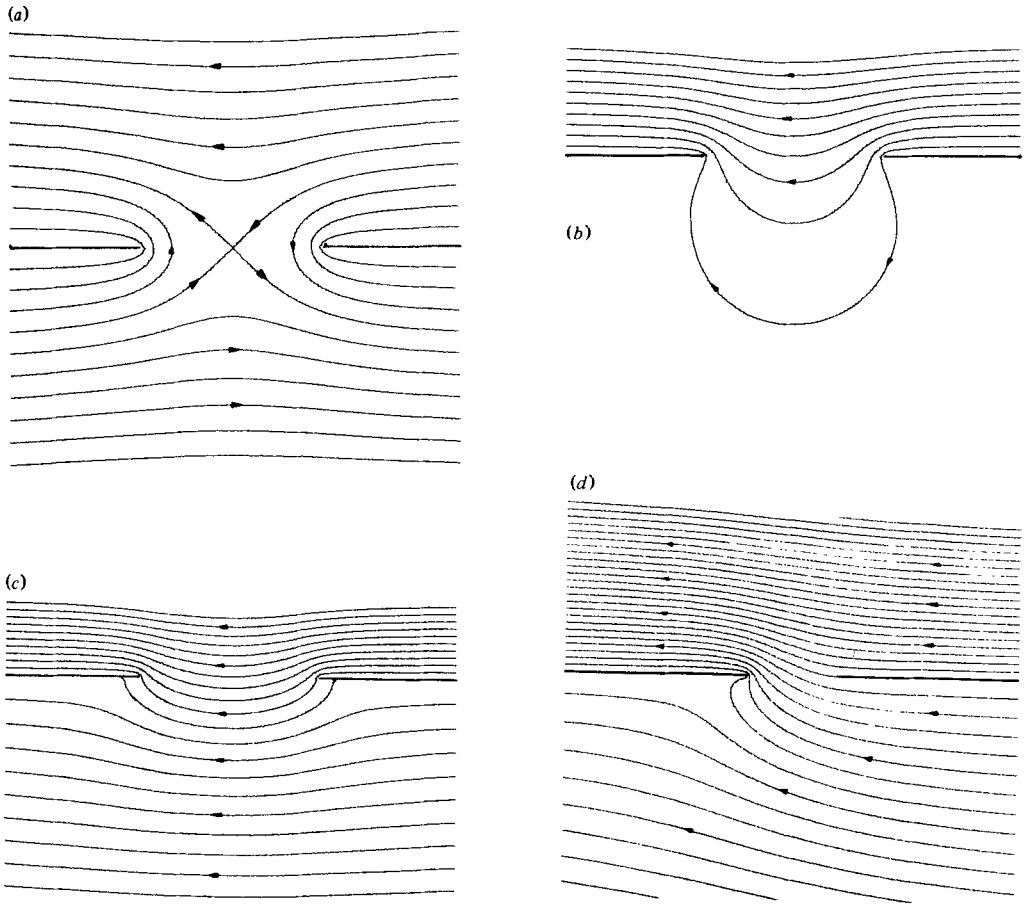

FIGURE 9. The flow near an aperture in a plane boundary: (*a*) with equal and opposite streams either side and no net flux through the aperture; (*b*) with stagnant fluid to one side and no net flux through the aperture; (*c*) with fluid of different velocities but in the same direction on either side, and no net flow through the aperture; (*d*) the flow of (*c*) modified by the addition of a flux through the aperture to remove the singularity on the upstream edge.

between a stream of velocity U_1 above the plane and a stream of velocity U_2 below the plane. Note that the constant A multiplying the only term which leads to a net flow through the gap is so far undetermined.

Each of the terms in equation (3.1) satisfies the boundary conditions on the plane exactly, and each is therefore a possible flow with this boundary. The first term is a uniform flow parallel to the boundary, and is not influenced by the presence of the gap. The second term describes the flow when the streams either side of the boundary are equal in magnitude but opposite in direction. A set of streamlines for such a flow is shown in figure 9 (*a*). There is a stagnation point in the middle of the gap, and the fluxes through the gap either side of this point are equal and opposite.

These first two flows may be combined to produce any pair of stream velocities required. Figure 9 (*b*) shows the streamlines for flow past a gap with stagnant fluid on the other side, while figure 9 (*c*) has different velocities both in the same direction either side. All of these flows satisfy the boundary conditions and equations of motion

without the third term in equation (3.1), so where does this term come in? If we look again at figure 9(*c*) we see that there are two symmetrically positioned stagnation points near the gap, and singularities at the edges of the gap. The flow off the upstream edge of the gap is similar to that at the trailing edge of a flat-plate aerofoil when the Kutta condition is not satisfied. For such an aerofoil, the attached circulation may be modified by vortex shedding to remove the singularity at the trailing edge. Similarly in the case of the flow past an aperture, we suggest that the physics of the flow will cause a flux through the gap sufficient to remove the singularity on the upstream plane. The flow will then leave this plane tangentially. When this condition is satisfied, which requires that $A = -\frac{1}{2}\delta(U_1 - U_2)$ in equation (3.1), the flow in figure 9(*c*) becomes that in figure 9(*d*).

There will still be a singularity on the edge of the downstream plane, just as there is always a singularity on the leading edge of the flat-plate aerofoil.

The above argument will only apply if the flow is in the same direction either side of the gap. If the flow is in opposite directions, then we cannot say that one plane is upstream and the other downstream of the gap. It could be argued that the flux through the gap is likely to be from the high pressure side to the low pressure side, which allows the removal of the singularity on the plane upstream of the gap with respect to the faster-moving fluid. The opposite flux would remove the singularity on the other plane. It seems reasonable to suggest that, whatever value the flux takes in practice, it will be of magnitude no greater than these limiting values, so, in equation (3.1),

$$|A| \leqslant \tfrac{1}{2}\delta|U_1 - U_2|. \tag{3.2}$$

The flux through the gap may be calculated from the complex potential, and is found to be $A\pi$. This is consistent with the observation that in the far field to one side of the gap the term representing the flux approximates to a simple source of strength $A\pi$ placed next to a plane boundary, and in the far field to the other side of the gap it approximates to a simple sink of equal strength.

We have now found a description of the flow that will result when a gap appears in a plane boundary between two streams of differing velocities. As would be expected, the flow velocities are only changed significantly within a region of the same order of linear dimension as the gap, though as shown in figure 9(*d*) the streamlines may be displaced by a distance of the same scale as the gap everywhere downstream of the gap.

To estimate the effect of the appearance of the gap on the rotor circulation we must see whether letting the size of the gap tend to zero results in the limit in the same flow as is generated when there is no gap. Equation (3.1) shows that this is the case if we include the fact that A is $O(\delta)$. Can the very small disturbance to the flow generated by an infinitesimal gap cause a finite change in the rotor circulation? Consider the contribution to the circulation from the section of the half-plane between (δ, O) and (x_1, O) on the positive real axis. The path for calculating the contribution is taken from $(x_1, i\epsilon)$ along just above the real axis to the origin and then back below the real axis to $(x_1, -i\epsilon)$. With no gap the integral of the velocity along the path is $x_1(U_2 - U_1)$. With a gap of width 2δ it becomes $(U_1 - U_2)\,(x_1^2 - \delta^2)^{\frac{1}{2}} - A \log[\delta^{-1}(x_1 + (x_1 - \delta^2)^{\frac{1}{2}})]$; letting $\delta \to 0$ with $A = O(\delta)$ gives the same result. It follows that the appearance of an infinitesimal gap does not affect the rotor circulation, and thereafter Kelvin's circulation

theorem ensures that no change can take place until the rotor makes contact with a subsequent stator.

It remains only to note that the addition of the small horizontal section to the rotor (AX in figure 8) has a small effect on the rotor circulation, in the sense that the change tends to zero with the size of the additional section. Thus it is reasonable to base our calculations on the original model as shown in figure 1 and to take the circulations immediately after blade separation to be the same as those just before.

4. Interacting cascades

We now know that a pair of interacting aerofoils can generate circulations comparable to those resulting from application of the Kutta condition. We wish to build the interaction into a turbomachinery stage, and estimate the performance in comparison with a conventional stage. The problem arises here that there are a large number of different parameters which will affect the results of the calculation. We have therefore chosen to base our calculations on a geometry close to that used in the experiments (see figure 10).

The stage used in the following calculations has rotor and stator blades which are flat plates of equal chord, with the blade spacing also equal to the chord. The conventional two-dimensional cascade representation is used with infinite blade sets along the x axis, and flow down the y axis representing axial inflow with no swirl. The blade staggers are 45° and 30° for the rotor and stator respectively. For the conventional cascade performance we have used the results of Weinig (1935) for the exact potential flow through a cascade of flat plates, the relevant sections of which are summarized by Horlock (1958). The rotor and stator are treated separately, though the entry conditions at the stator are of course determined by the flow deflexion through the rotor.

The interacting cascade results were obtained by treating each rotor–stator interaction in isolation. The blade circulations were calculated by methods outlined earlier, and the rotor blade lift was assumed to be that resulting from the movement of this circulation relative to the inflow. The rotor circulation also causes a deflexion of the main stream which will then generate lift on the stator. Since the rotor and stator circulations are equal, the outflow from the stator will be axial, at least outside the disturbed area.

It is worth noting here that, since the rotor and stator circulations are equal but opposite in sign, when the blades touch subsequently the total circulation on each rotor–stator pair will be zero, as we assumed for the starting condition, so the solution does represent the steady state.

In any machine working in a real fluid, the generation of excess circulation over that required by the Kutta condition would result in vortex shedding and gradual return to the Kutta level. Each interaction would then return the circulations to their high value, so the mean circulation would be above the Kutta value. Thus we should expect a real machine to work somewhere between these two possible conditions; the calculation of the actual level is beyond the scope of this paper. It is expected that an approach like that of Kemp & Sears (1953) would give an approximation to the mean flow conditions.

The results of these calculations are presented in figures 11 and 12. Figure 11 gives

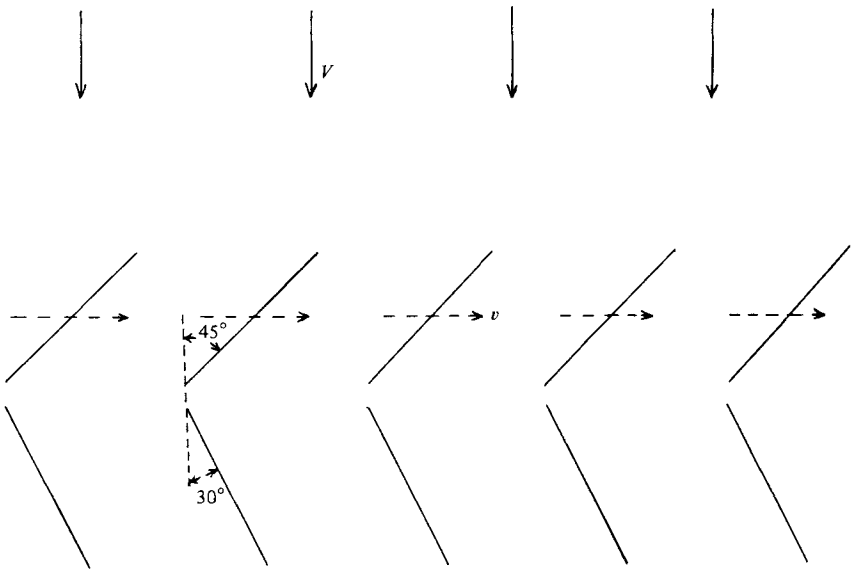

FIGURE 10. The geometry used for the stage calculations.

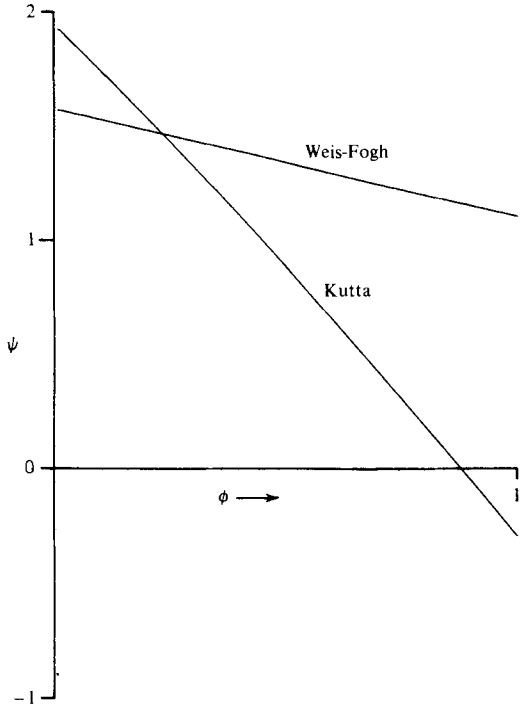

FIGURE 11. The overall performance of a stage operating under Kutta or Weis-Fogh conditions. The stage loading ($\psi = \Delta p/\frac{1}{2}\rho v^2$) is shown against flow coefficient ($\phi = V/v$).

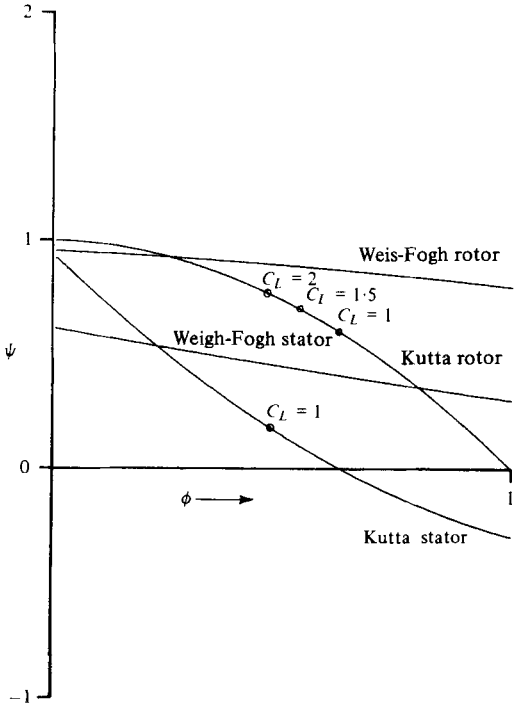

FIGURE 12. The rotor and stator stage loadings ($\psi = \Delta p/\frac{1}{2}\rho v^2$) for flow coefficients ($\phi = V/v$) between 0 and 1. The lift coefficients are shown for the Kutta blading to indicate where stall may be expected.

the stage loading ($\Delta p/\frac{1}{2}\rho v^2$, where Δp is the pressure rise and v the rotor velocity) against the flow coefficient (V/v, V being the axial fluid velocity). Figure 12 breaks the total stage loading down into separate rotor and stator loadings. We have also marked on figure 12 the lift coefficients of the conventional rotor and stator at various loading conditions, to give some impression of where stall will occur, since our calculations do not allow for flow separation. The results show that the interaction blading has a very similar performance to the conventional blading at the peak operating condition, but the stage pressure rise reduces much more slowly as the flow increases. Thus the interaction stage may be expected to produce useful pressure rises over a significantly wider range of operating conditions. The relative peak performance may vary from one geometry to another, but in the case considered here the interaction stage appears to produce a somewhat higher pressure rise.

It should be said here that our potential flow models do not enable us to make any estimate of the relative efficiencies of the two stages, and for many applications the efficiency is at least as important as the stage pressure rise. Realistic estimates of the effect of the interaction on efficiency are most easily found by experiment, and we shall now describe the results of our initial tests.

The experiments were performed on a small closed-cycle water rig at the Whittle Laboratory, Cambridge. The working section of the apparatus was modified to allow the axial separation of a conventional stage to be varied by means of metal shims. The rig allowed for the measurement of static pressure rise and overall efficiency of the

Rotor	chord	20 mm
	profile	10C4 on circular arc
	camber	30°
	stagger	45°
Stator	chord	20 mm
	profile	10C4 on circular arc
	camber	30°
	stagger	30°
Both blade sets	material	polycarbonate
	hub diameter	66 mm
	tip diameter	88 mm
	tip clearance	0·1 mm nominal
Rotor-stator clearances		0·1 to 5 mm
Flow rates		5 to 13 kg s^{-1}
Rotor speed		2500 r.p.m.

TABLE 1. Details of tested stage.

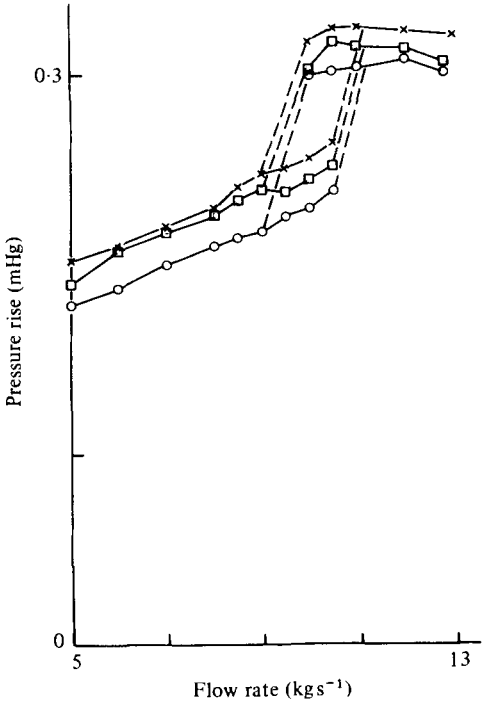

FIGURE 13. The stage pressure rise. Separation (mm): ×, 0·1; □, 0·3; ○, 2·5.

stage. The blades had a chord of 20 mm, and the rotor–stator separation was varied between 5 mm, representing a conventional arrangement, and around 0·1 mm, which was as close to contact as the equipment would allow. Further blading details are given in table 1.

The results of the tests are shown in figures 13 and 14. Figure 13 shows the overall stage pressure rise, which demonstrates an increase in pressure rise with decreasing

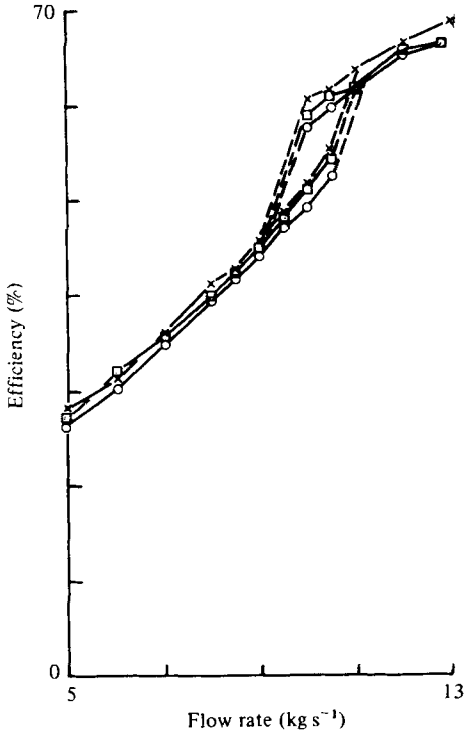

FIGURE 14. The stage efficiency. The symbols are the same as in figure 13.

separation of 5 to 10 % both above and below the stalling point. The efficiency (figure 14) also shows an improvement, but to a lesser extent. Thus our calculations suggest that there may be significant performance advantages in using a high interaction stage in a turbo-machine, and our initial experiments have demonstrated an increase in stage loading with no increase in losses when the rotor–stator interaction is increased.

It is worth commenting here that performance improvements have been observed in several jet engine axial compressors as a result of reducing the axial separation of blades. Miller (1971) reviews the relevant engine test results. The clearances in these tests are not sufficiently small to result in an approximate rotor–stator seal at any instant, but viscous effects must ensure a certain degree of blocking with reduced separation, which will in turn lead to an interaction similar to that presented earlier in this paper.

5. Conclusion

Recent studies of animal hovering motions have revealed a method of lift generation not previously considered by aerodynamicists. The insects that use the process achieve a lift coefficient double that achieved by animals that use a conventional vortex-shedding process. We have attempted to demonstrate that the principle of the new

(to aerodynamicists, but not insects!) process may have engineering applications. Furthermore, being radically different in principle from that used in conventional aerodynamics, it might well offer some performance advantage.

We have suggested a design for an axial flow compressor using the new process, and shown how a simple model of this design may be analysed mathematically. The results show that the effect is strong enough to be of interest to designers of machines.

The effect of varying levels of interaction in axial flow stages has been investigated experimentally. The results show a measurable improvement in performance as the interaction is increased, and we suggest that the improvement may well be due to the effect illustrated by the theoretical model.

Weis-Fogh (1973) and Lighthill (1973) have explained the novel mechanism used by the insect to enhance its aerodynamic performance, and much interest has been shown by aerodynamicists in their work. We suggest that this interest should now be extended to a serious consideration of the application of the mechanism to the solution of engineering problems.

One of us (S B F) gratefully acknowledges the support of an SRC research studentship and the opportunities afforded by the Rolls-Royce Research Fellowship at Emmanuel College, Cambridge.

REFERENCES

ABRAMOWITZ, M. & STEGUN, I. A. 1964 *Handbook of Mathematical Functions*. Washington, National Bureau of Standards.

BATCHELOR, G. K. 1967 *An Introduction to Fluid Dynamics*. Cambridge University Press.

COESTER, R. 1959 *Theoretische und experimentelle Untersuchungen an Querstromgebläsen*, vol. 28. Zürich: Leeman.

HORLOCK, J. H. 1958 *Axial Flow Compressors*. Butterworth Publications Ltd.

JEFFREYS, H. & JEFFREYS, B. S. 1956 *Methods of Mathematical Physics*. Cambridge University Press.

KEMP, N. H. & SEARS, W. R. 1953 *Aero. Sci.* **20**, 585–597.

LIGHTHILL, M. J. 1973 *J. Fluid Mech.* **60**, 1–17.

MILLER, D. C. 1971 The effect of axial gaps on compressor performance. *Rolls-Royce Ltd. int. publ. ref. no.* G.N. 14229.

WEINIG, F. 1935 *Die Strömung um die Schaufeln von Turbomachinen*. Leipzig: Joh Ambr. Barth.

WEIS-FOGH, T. 1973 *J. Exp. Biol.* **59**, 169–230.